Effect of Brine Composition on CO_2/Limestone Rock Interactions during CO_2 Sequestration

Ibrahim Mohamed[*1],Jia He[2],and Hisham A. Nasr-El-Din[3]

[1]Advantek International Corp. [*]*Formerly with Texas A&M University*

Houston, Texas, USA 77063.

[2, 3]Texas A&M University, Petroleum Engineering Department
College Station, Texas, USA 77843

[*1]IMohamed@ADVNTK.com; [2]Jia.He@PE.TAMU.edu; [3]Hisham.Nasreldin@PE.TAMU.edu

Abstract

Several parameters affect the chemical reactions between CO_2/fluid/rock: pressure, temperature, rock type, and brine composition. Brine composition includes salt concentration and type. Pink Desert limestone cores were used to conduct a series of coreflood experiments to address the effect of brine composition on the chemical reactions between carbonic acid and limestone rock.

The experiments were designed to simulate the water alternating gas (WAG) injection of CO_2 into saline carbonate aquifers. Supercritical CO_2 and brines were injected at flow rates of 2 and 5 cm^3/min at 70 and 200°F. Seawater, formation brine, calcium chloride, sodium chloride, and magnesium chloride brines were used in this study.

A commercial compositional simulator was used to simulate the coreflood experiments at the lab conditions. The reaction rate constant of CO_2 with calcite at different brine compositions was adjusted to match the calcium concentration obtained in the lab.

Experimental data was used to predict the reaction rate constant between CO_2/brine/rock and found to be increasing as the brine salinity increased ($Log(k_{25})$= -9.2) when CO_2 dissolves in DI water, and -6.2 when CO_2 dissolves in 5 wt% $CaCl_2$ brine). A simulation study conducted on field scale showed that after 30 years of CO_2 injection and 1400 years after injection stopped, brine composition does not affect the trapping mechanism of CO_2 in the aquifer.

Keywords

CO_2 Sequestration; Coreflood Experiments; CO_2 Injection Modeling; CO_2/Brine/Rock Chemical Reactions

Introduction

The primary factor affecting well performance during CO_2 injection is rock type (carbonate or sandstone). For example, solution channels can be formed in limestone, creating a dominant flow path significantly altering flow behaviour (Grigg and Svec 2008). Increases in Ca^{2+}, Mg^{2+}, HCO_3^-, and CO_2 concentrations were noticed during monitoring, and the produced aqueous fluids and gases confirms the dissolution effect noted during CO_2 injection (Raistrick et al. 2009). Brine salinity and composition play a key role in the chemical reaction between CO_2/water/rock during CO_2 sequestration, since the total dissolved solids (TDS) affects the solubility of CO_2 in brines.

CO_2 is an acidic gas that dissolves in formation brine forming weak carbonic acid. Carbonic acid dissolves carbonate rocks forming calcium bicarbonate ($Ca(HCO_3)_2$). When the formation brine or the displacement brine contains SO_4^{2-}, calcium sulfate can precipitate (Egermann et al. 2005).

Krumhansl et al. (2002) concluded that with continuous dissolution of calcite, calcium saturation will increase and calcium sulfate precipitation will take place inside the core. This kind of precipitation is temperature dependent. At temperatures lower than 40°C, gypsum is the stable form, while at higher temperatures, anhydrite is the stable product. Hemihydrate is a metastable phase (Meijer and Van Rosmalen 1984).

The objective of this paper is to study the effect of brine composition on the chemical reactions between CO_2 and the formation lithology during WAG injection of CO_2 into a limestone aquifer. Furthermore, the impact of flow rate and temperature, on the final permeability has been studied. NaCl, $CaCl_2$, and $MgCl_2$ were tested at various concentrations (0, 1, 5, and 10 wt%). The reaction kinetics were obtained using a compositional simulator CMG-GEM (Generalized Equation-of-State Model) for each brine used in the current study.

Solubility of Calcium Sulfate

Solubility of calcium sulfate in brines is mainly controlled by the molecular hydration state. The solubility is also affected by temperature and brine salinity. The first solubility plot of calcium sulfate was published by Partridge and White (1929); their results showed that the solubility of anhydrite and hemihydrate in distilled water decreases as temperature increases. While gypsum solubility in distilled water increases as temperature increases up to 38°C, at higher temperatures solubility of gypsum decreases as temperature increases.

Meijer and Van Rosmalen (1984) used a computer program developed by Marshall and Sulsher (1968) to calculate the solubility of calcium sulfate in seawater. Their results showed that the solubility in seawater is higher than the solubility in distilled water, although temperature has the same effect on the solubility of calcium sulfate for both cases. Solubility of calcium sulfate decreases significantly as the total dissolved solid content approaches twice than that of seawater (Flint 1967).

Solubility of CO_2 in Brines

The effect of dissolved solids on the CO_2 solubility in water was studied by Enick and Klara (1989). They developed a correlation to calculate the solubility of CO_2 in brine that is applicable at reservoir conditions, taking into consideration the effect of dissolved solids. They assumed that solubility only depended on TDS, regardless of the type of salt.

The solubility of CO_2 in distilled water, NaCl and $CaCl_2$ brines used in the present study, at a pressure of 1300 psi and temperature of 200°F, was obtained from Nighswander et al. (1989), Duan et al. (2006), and Prutton and Savage (1945). Their work was specified for NaCl and $CaCl_2$ brines, while the solubility of CO_2 in $MgCl_2$ brines was calculated using the equation developed by Enick and Klara (1989) and is given in Table 1.

TABLE 1 CO_2 SOLUBILITY AT 1300 PSI AND 200°F

Salt Concentration, wt%	**0**	**1**	**5**	**10**
Brine Composition	**CO_2 Solubility, weight fraction**			
NaCl	0.0134	0.0130	0.0115	0.0098
$CaCl_2$		0.0130	0.0115	0.0096
$MgCl_2$		0.0128	0.0105	0.0083

Reaction Kinetics

The rate laws for mineral dissolution and precipitation for the chemical reactions between CO_2/brine/limestone are (Bethke 1996):

$$r_\beta = k_\beta A_\beta \left[1 - \left(\frac{Q_\beta}{K_\beta}\right)\right] \quad (1)$$

$$k_\beta = k_{0\beta} \exp\left[-\frac{E_{a\beta}}{R}\left(\frac{1}{T} - \frac{1}{T_0}\right)\right] \quad (2)$$

Where;

A_β = reactive surface area for mineral β, m²
$E_{a\beta}$ = activation energy for reaction of CO_2 with mineral β, J/mol
K_β = chemical equilibrium constant
$k_{0\beta}$ = rate constant of reaction of CO_2 with mineral β at a reference temperature T_0, mol/m².s
k_β = rate constant of reaction of CO_2 with mineral β at temperature T, mol/m².s
Q_β = ion activity product
R = universal gas constant = 8.31 J/mol.°K
r_β = Reaction rate, mole/m².s
T = temperature, °K

TABLE 2 LIST OF KINETIC RATE PARAMETERS FOR REACTIONS BETWEEN CO_2 AND LIMESTONE

Reference	**Log(ko) mol/m².sec**	**Ea KJ/mol*°K**	**Reference Temperature °C**	**Brine Composition**	
				Ion	**Conc. mg/l**
Gaus et al. (2004)	-6.35		37	Al	9.47E-04
				Ba	1.72
				C	0.83
				Ca	7093.88
				Cl	16982.08
				Fe	0.02
				K	5.55
				Mg	269.79
				Na	2436.92
				S	15.42
				Si	7.08
Bacon et al. (2009)	-1.69	23.5	54	Na	55152.53
				Mg	3038.13
				Al	0.01
				SiO_2	7.21
				K	18258.91
				Ca	30240.00
				Mn	2.20
				Fe	0.56
				Cl	125007.98
				SO_4	158.50
				HCO3	134.24
Sorensen et al. (2009)	-6.19	62.76	25	10 wt% NaCl	
Lee and Morse (1999)	-8.94		25	Na	91.60
				Ca	40.00
				Cl	141.37
				HCO_3	122.00

Reference	Log(ko) mol/m².sec	Ea KJ/mol*°K	Reference Temperature °C	Brine Composition	
				Ion	Conc. mg/l
Wellman et al. (2003)	-2.00		25	Na	16,575.65
				SO_4	629.21
				Mg	631.93
				Cl	29,993.41
				Ca	1,824.00
Knauss et al. (2005)	-6.19	62.7	25	Al	8.70E-04
				Ba	59.18
				Sr	109.44
				Ca	2,211.64
				Fe	36.28
				K	414.21
				Mg	461.82
				Na	40,845.98
				SiO_2	24.11
				Cl	68,757.94
				SO_4	10.32
Cantucci et al. (2009)	-5.81	23.5	25	Na	42,990.93
				K	2,502.29
				Ca	39.48
				Mg	0.16
				HCO_3	447.25
				Cl	63,815.76
				HS	3,261.04
				SO_4	4.44
				Li	2.57
				Sr	46.88
				Si	10.44
				Al	1.84E-03
Xu et al. (2006)	-6.19	62.76	25	Ca	7,284.00
				Mg	112.05
				Na	27,886.63
				K	2,807.26
				Fe	0.08
				Cl	60,979.50
				SiO_2	210.30
				HCO_3	457.63
				SO_4	194.05
				Al	1.53E-04
				Pb	2.07E-07
Wigand et al (2009)	-1.69	23.5	25	Al	0.08
				SiO_2	4.27
				Ca	275.48
				Fe	17.98
				K	64.00
				Mg	39.01
				Mn	47.03
				Zn	1.83
				Li	0.02
				Sc	0.16
				Cu	0.95
				Rb	0.07
				Sr	0.44
				Cd	0.02
				Pb	0.02

Different values for k_o between carbonic acid and calcite were reported in the literature (Alkattan et al. 1998). A summary of k_o and E_a used in previous studies with different brine compositions is given in Table 2. Log(k_o) ranged from -8.94 at a low salinity brine with TDS of 395 mg/l (Lee and Morse 1999), to -1.69 for a high salinity formation brine with TDS of 232,000 mg/l (Bacon et al. 2009).

Experimental Studies

Materials

Cylindrical Pink Desert limestone cores were used in this study with dimensions of 6 in. length and 1.5 in. diameter. the cores permeability and porosity are summarized in Table 3.

TABLE 3 PROPERTIES OF THE PINK DESERT CORES AND COREFLOOD EXPERIMENTS

Core #	Porosity (vol%)	Perme-ability (mD)	Temp-erature (°F)	Injection flow rate of CO_2 and brine (cm^3/min)	Brine Injected
1	19.6	61.8	200	2	Seawater without Sulfate
2	21.9	50.0	200	2	Seawater
3	18.9	56.52	70	2	Seawater
4	19.8	79.8	200	5	Seawater without Sulfate
5	22.4	77.0	200	5	Seawater
6	22.4	68.2	200	2	Formation Brine
7	19.6	57.5	70	2	Formation Brine
8	27.1	96.0	200	5	Distilled Water
9	24.1	77.0	200	5	1 wt% NaCl
10	24.4	99.0	200	5	5 wt% NaCl
11	24.4	99.0	200	5	10 wt% NaCl
12	25.9	93.5	200	5	1 wt% $CaCl_2$
13	24.7	91.0	200	5	5 wt% $CaCl_2$
14	26.9	85.0	200	5	10 wt% $CaCl_2$
15	26.2	80.0	200	5	1 wt% $MgCl_2$
16	23.6	72.0	200	5	5 wt% $MgCl_2$
17	24.8	93.0	200	5	10 wt% $MgCl_2$

CO_2 with purity of 99.8% (the impurities were mainly water vapor and nitrogen) was used in this study. Different synthetic brines were used; 1) equivalent to seawater excluding Na_2SO_4, 2) equivalent to seawater, and 3) equivalent to formation brine from the Middle East. The compositions of the three brines are given in Table 4. Bines that are composed of NaCl, $MgCl_2$, or

$CaCl_2$, at concentrations of 1, 5, and 10 wt% were also used. The density of the different brines were measured at room temperature using a DMA4100 density meter, and a PSL 1643/02 capillary viscometer was used to measure brine viscosity.

Coreflood Experiments

Seventeen coreflood experiments were conducted in this study. The experiments were run at temperatures of 70 and 200°F, and injection flow rates of 2 and 5 cm^3/min were used. A summary of the coreflood experiments is given in Table 3. More information about the coreflood setup was reported previously (Mohamed and Nasr-El-Din 2012).

TABLE 4 CONCENTRATIONS OF KEY IONS AND PROPERTIES OF SYNTHETIC BRINES

Ion	Seawater Without Sulfate	Seawater	Formation Brine
Cl^-	22,010*	22,010	143,285
SO_4^{2-}	0	2,850	108
Na^+	12,158	12,158	51,187
Mg^{2+}	1,315	1,315	4,264
Ca^{2+}	401	401	29,760
TDS, mg/l	35,884	38,734	228,604
Viscosity**, cP	1.040	1.045	1.70
Density**, g/cm^3	1.0260	1.0266	1.1640

*all concentrations are expressed in mg/l.
** measured at 70°F
pH ranges 6.4 to 6.9

Coreflood Procedure

1- The cores were dried in an oven at a temperature of 257°F for 5 hours, and then weighed.
2- The cores were saturated under vacuum with brine (brine composition depends on the experiment), and then weighed.
3- From the weight difference between the dry and saturated core and the brine density, the core porosity was calculated.
4- A core was placed inside the coreholder and brine was injected at room temperature until the pressure drop across the core stabilized. The core permeability was calculated using Darcy's law.
5- The system was heated up to the required temperature.
6- Start CO_2 injection at a constant flow rate for 5 pore volumes (CO_2 half cycle).
7- Alternate to brine for 5 pore volumes (brine half cycle).
8- Repeat steps 6 and 7 to reach the 3 WAG cycles.
9- Core effluent samples were collected throughout the experiment.
10- The concentrations of calcium, sodium, and magnesium ions were measured in the core effluent samples. Sulfate ion was measured when seawater was used.
11- A new core was used in each experiment.

Equipment

Calcium, sodium, and magnesium concentrations in the core effluent samples were measured using an AAnalyst 700-flame type. Sulfate concentration was measured using an Orbeco SP600 Spectrophometer, using the turbidity method based on precipitation with barium chloride.

Results and Discussion

WAG injection of CO_2 and seawater was conducted on cores #1-2 (seawater not containing sulfate for core #1, seawater with sulfate for core #2). Calcium concentration noted for core #1 was higher than the calcium concentration measured in the core effluent samples collected for core #2. Also, a reduction in the sulfate concentration was noted for core #2, which indicated that calcium sulfate precipitation occurred inside core #2.

Total amounts of calcium collected from cores #1 and 2 were 0.64 and 0.45 g, respectively, and the weight of the sulfate lost inside core #2 was 0.08 g (5.3% of the total weight of the injected sulfate). More damage was noted for core #2 because of calcium sulfate scales precipitated inside the core (permeability reduced from 50 to 43 mD). The change in the permeability for core #1 was negligible.

Effect of Temperature

Two temperatures (70 and 200°F) were tested to address the effect of calcium sulfate hydration form. Gypsum is the stable form at 70°F, and anhydrite is the stable form at 200°F. Fig. 1 shows that at 70°F (core #3) a higher calcium concentration was noted in the core effluent sample compared to core #2 (200°F). The solubility of gypsum at 70°F was found to be higher than the solubility of anhydrite at 200°F, 0.42 wt% for gypsum and 0.195 wt% for anhydrite (Flint 1967; Linnikov and Podbereznyi 1996), which explains the

higher concentration of sulfate noted for core #2 (the precipitation was less).

At the two temperatures examined in this study, the results showed that at the lower temperature (70°F) the solubility of calcium sulfate and CO_2 in seawater is higher, and more calcium carbonate dissolved, which resulted in an increase in the core permeability (from 56.5 to 60.6 mD). At the higher temperature (200°F) the solubility of calcium sulfate and CO_2 in seawater is less, which caused more precipitation and less calcium carbonate dissolution, which resulted in more damage noted to the core.

Effect of Injection Flow Rate

In this study, two flow rates were examined, 2 and 5 cm^3/min. A flow rate of 2 cm^3/min was discussed briefly in the previous section. Two coreflood experiments run at 5 cm^3/min, core #4 was run with no sulfate in the injected brine, and core #5 with sulfate in seawater composition, both were conducted at 200°F.

The injection flow rate of CO_2 did not have a significant effect on the core permeability after WAG injection of CO_2. The same behavior was noted when CO_2 was injected at 2 and 5 cm^3/min. Maximum calcium and minimum sulfate concentrations were similar at injection flow rates of 2 and 5 cm^3/min (Fig. 1). Precipitation of calcium sulfate was also evaluated by the change in the core permeability. For core #5, the permeability decreased from 77 to 69 mD; while it increased from 79.8 to 83 mD for core #4.

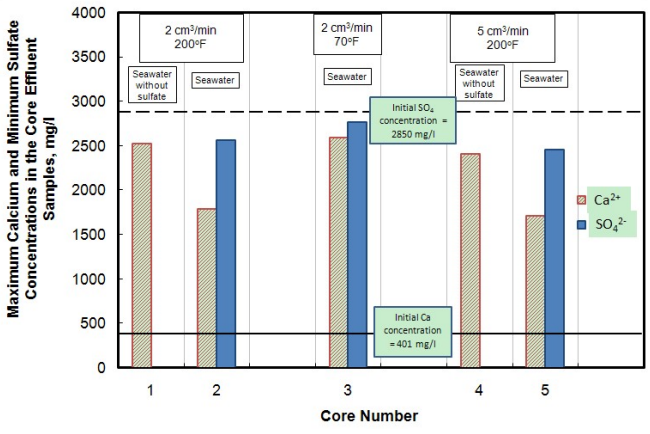

FIG. 1 MAXIMUM CALCIUM AND MINIMUM SULFATE CONCENTRATIONS IN THE CORE EFFLUENT SAMPLES FOR CORES #1-5

Effect of the High Salinity Formation Brine

Cores #6 and 7 were both flooded with CO_2 alternating formation brine at two different temperatures (70 and 200°F), the total dissolved solids for the formation brine used in this study was 228,604 mg/l (Alotaibi et al. 2010)

Fig. 2 shows that the increase in calcium concentration when formation brine is used in WAG injection is more pronounced when compared to seawater injection with CO_2. Calcium concentration increased from 29,760 mg/l initially to a maximum concentration of 60,000 mg/l during CO_2 injection at 200°F, and increased to 42,000 mg/l at 70°F.

The formation brine originally has low sulfate concentration, so the effect of the calcium sulfate scale was insignificant. The damage was mainly because of calcium carbonate precipitation as the calcium concentration noted in the core effluent sample was very high. Permeability of core #6 decreased from 68.2 to 64 mD, while for core #7, it increased from 57.5 to 63 mD.

Table 5 summarizes the change in the cores permeability, and Fig. 3 gives a brief summary of the total calcium collected in the core effluent samples and total sulfate precipitated for each experiment for cores #1-7.

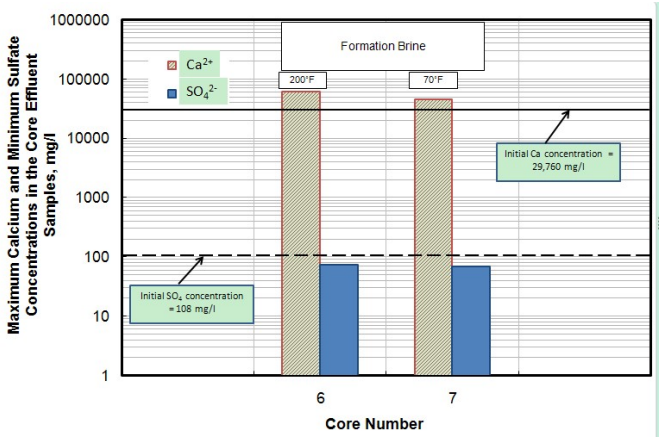

FIG. 2 MAXIMUM CALCIUM AND MINIMUM SULFATE CONCENTRATIONS IN THE CORE EFFLUENT SAMPLES FOR CORES #6-7

Effect of Brine Salinity

Effect of Deionized Water (DI Water)

Calcium concentration increased during CO_2 injection from 0 to 1080 mg/l due to rock dissolution, and a reduction in calcium concentration was observed during water injection to 500 mg/l. This behavior was repeated each cycle, with a slight change in the calcium concentration values. The maximum values were 1184 and 1070 mg/l, and the minimum values were 300 and 530 mg/l for the second and third cycles, respectively.

The total calcium collected from core #8 was 0.353 g. A reduction in the core permeability from 96 to 90 mD was observed after CO_2 injection.

Effect of NaCl Brines

Three coreflood experiments were run at NaCl concentrations of 1, 5, and 10 wt%. Measuring the permeability for these cores before and after CO_2 injection, showed no significant change in core permeability.

For 1 wt% NaCl brine, the maximum calcium concentration was almost the same as when distilled water was used (Fig. 4). The minimum calcium concentrations were 300 and 1000 mg/l for distilled water and 1 wt% NaCl brine, respectively. The maximum calcium concentrations were 1276, 1841, and 1700 mg/l, while the total calcium collected was 0.436, 0.635, and 0.54 g for 1, 5, and 10 wt% NaCl brine, respectively.

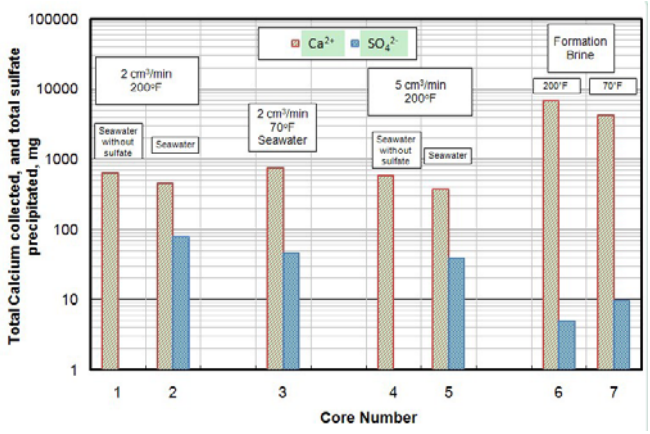

FIG. 3 TOTAL CALCIUM COLLECTED AND TOTAL SULFATE LOSS AS MEASURED IN THE CORE EFFLUENT SAMPLES.

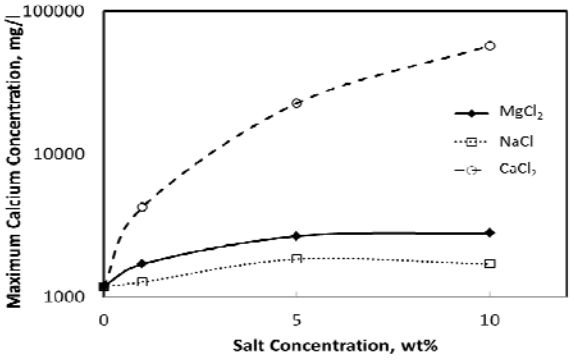

FIG. 4 MAXIMUM CALCIUM CONCENTRATION IN THE CORE EFFLUENT SAMPLES.

Effect of $CaCl_2$ Brines

Fig. 4 shows that for 1 wt% $CaCl_2$ brine, the maximum calcium concentration increased from 3100 mg/l initially to 4256 mg/l. This was an increase of 1156 mg/l, which was equal to the increase of calcium concentration when distilled water was used.

A significant increase in the calcium concentration in the core effluent samples was observed when increasing the concentration of calcium chloride in the injected brine. For 5 wt% $CaCl_2$ brine the calcium increased from 15,504 to a maximum concentration of 22,792, with a 7,288 mg/l increase in calcium concentration. When doubling calcium chloride concentration to 10 wt%, calcium increased from 31,008 to 57,000 mg/l, with 26,000 mg/l increase in calcium concentration. The total collected amounts of calcium were 0.32, 2.44, and 6.17 g for 1, 5, and 10 wt% $CaCl_2$ brine, respectively.

The ratio of the final core permeability to the initial permeability is given in Fig. 5. An enhancement in core permeability, of 6.5 %, was noted when 1 wt% $CaCl_2$ brine was injected, compared to 7 % loss in permeability when distilled water was used. At higher calcium chloride concentrations, 5 and 10 wt%, a permeability reduction of 14 % occurred after WAG injection of CO_2.

TABLE 5 EFFECT OF BRINE COMPOSITION ON THE CORE PERMEABILITY AFTER CO_2 WAG INJECTION

Core	$K_{initial}$ (mD)	K_{final} (mD)	Ratio	Injection Conditions	Brine
1	61.8	60.5	0.98	2 cm³/min 200°F	Seawater without sulfate
2	50	43	0.86		Seawater
3	56.5	60.6	1.07	2 cm³/min 70°F	Seawater
4	79.8	83	1.04	5 cm³/min 200°F	Seawater without sulfate
5	77	69	0.90		Seawater
6	68.22	64	0.94	200°F	Formation Brine
7	57.5	63	1.1	70°F	

A. *Effect of $MgCl_2$ Brines*

To examine the effect of magnesium chloride concentration on the core permeability during CO_2 sequestration, three coreflood experiments were run. Fig. 4 shows that with increasing the concentration of $MgCl_2$ in the injected brine, more calcium was collected in the core effluent samples. The maximum concentration of calcium detected in the samples were 1764, 2686, and 2843 mg/l for 1, 5, and 10 wt% $MgCl_2$

brine, respectively. Total amount of calcium collected was 0.477, 0.687, and 0.956 g. Magnesium concentration was the same for all core effluent samples.

Fig. 5 shows that as magnesium chloride concentration increased, the damage introduced to the cores was still close: 4, 5, and 8 % loss in the core permeability for 1, 5, and 10 wt% $MgCl_2$ brine, respectively.

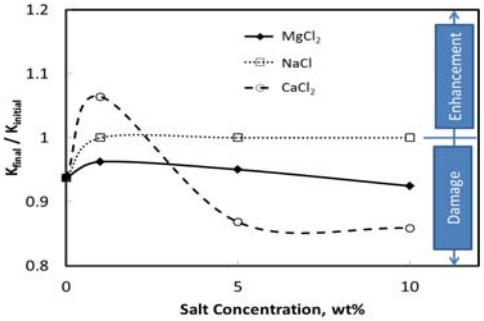

FIG. 5 CHANGE IN CORES PERMEABILITY WHEN DIFFERENT SALT CONCENTRATIONS OF NACL, $MgCl_2$, AND $CaCl_2$ BRINE WERE INJECTED IN CO_2 WAG INJECTION.

Simulation Studies

The experimental results showed that the kinetics of the reaction between CO_2 and limestone rock is a function in the brine composition. A compositional simulator (CMG-GEM) was used to predict the reaction rate constant between CO_2 and limestone for each brine used based on the calcium concentration measured in the core effluent samples. A field scale simulation was also run to address the effect of brine composition on the permeability distribution during WAG injection of CO_2.

The simulator input is: the injection schedule, CO_2 and brine relative permeability curves, capillary pressure between CO_2 and injected brine, kinetics of the chemical reactions between CO_2 and calcite, initial porosity and permeability, and the core dimensions.

To calculate the relative permeability curves, the irreducible water saturation and the critical saturation of CO_2 were obtained from the coreflood experiments. Relative permeabilities were calculated using Equations (3) and (4);

$$k_{rw} = 0.35\left(\frac{S_w - 0.25}{1 - 0.25}\right)^4 \quad (3)$$

$$k_{rCO2} = 0.05\left(\frac{S_{CO2} - 0.15}{1 - 0.15 - 0.25}\right)^{1.5} \quad (4)$$

Where;

k_{rw} = relative permeability to brine

k_{rCO2} = relative permeability to CO_2

S_w = brine saturation

S_{CO2} = CO_2 saturation

0.35 = relative permeability to brine at irreducible CO_2 saturation

0.05 = relative permeability to CO_2 at irreducible brine saturation

0.25 = irreducible brine saturation

0.15 = irreducible CO_2 saturation

The capillary pressure between CO_2 and brine was obtained using the model developed by El-Khatib (1995);

$$P_c = \frac{1}{\sqrt{2\tau}}\left(\frac{1}{\sqrt{2b+1}}\right)\left(\frac{(1-S_{wi})^{b+0.5}}{(S_w - S_{wi})^b}\right)\left(\frac{\sigma \ Cos\theta}{\sqrt{k/\phi}}\right) \quad (5)$$

Where;

B = saturation exponent

K = absolute permeability, m^2

P_c = capillary pressure, Pa

S_w = brine saturation

S_{wi} = irreducible brine saturation

T = tortuosity

Θ = contact angle

Σ = interfacial tension between CO_2 and brine, N/m

ϕ = porosity, fraction

El-Khatib (1995) gave an average value for the saturation exponent (b) to be 1.077. The tortuosity value was calculated based on the core porosity Equation (6) (Boving and Grathwohl 2001):

$$\tau = \varnothing^{-1.2} \quad (6)$$

Shariat et al. (2012) conducted a lab study to measure the interfacial tension between CO_2 and different brines, and the interfacial tension between CO_2 and seawater at the experimental conditions was found to be 0.0224 N/m. The contact angle between CO_2 and brine was adjusted in order to match the experimental results. Contact angle of 80° was found to give the best match for all cores used in the current study.

Core Scale Simulation

The cylindrical cores were divided into radial grids with 5X20X20 blocks in the radial coordinates r, Θ, and z directions, respectively. The initial permeability and porosity were assumed constant for all grid blocks, cores initial porosity and permeability are shown in Table 3.

The simulator uses Equations (1) and (2) to predict the dissolution and/or precipitation rate for calcium carbonate during the reaction with CO_2. In this paper, the activation energy of 62.7 KJ/mole.°K, and a reactive surface area of 9.5 cm^2/g were used for all cases (Svensson and Dreybrodt 1992). In order to simulate the calcium concentration obtained from the experimental study, the reaction rate constant was found ($\log(k_{25})$) to be in the range between -9.2 (for DI water case) and -6.2 (for 5 wt% $CaCl_2$ brine case). A summary for the reaction rate constant for all cases is given in Table 6. It is clear that at a higher salt content the reaction rate constant increases, and a larger value obtained for $CaCl_2$ brines than $MgCl_2$ brines, and a smaller value obtained for NaCl brines. The simulation failed at high calcium concentration cases (10 wt% $CaCl_2$ and formation brine), no reaction rate constant could be predicted for these cases.

The simulator also has the capability to predict the change in cores permeability due to the dissolution and precipitation reactions. The change in core porosity was calculated using Equation (7), while the permeability was calculated using Carman-Kozeny equation based on the initial and final porosity Equation (8):

$$\phi \equiv \phi_o - \sum_{\beta=1}^{n_m} \left(\frac{N_\beta}{\rho_\beta} - \frac{N^0{}_\beta}{\rho_\beta} \right) \quad (7)$$

$$k = k_o \left(\frac{\varphi}{\phi_o} \right)^m \left(\frac{1-\phi_o}{1-\phi} \right)^2 \quad (8)$$

Where;

K = Current permeability, mD
k_0 = Initial permeability, mD
m = Carman-Kozeny exponent
N_β = total moles of mineral β per bulk volume at the current time, mole/cm^3
$N^0{}_\beta$ = total moles of mineral β per bulk volume at the time 0, mole/cm^3
ϕ = Current porosity, fraction
ϕ_0 = Initial porosity, fraction
ϱ_β = mineral molar density, mole/cm^3

The permeability and porosity change distribution across the core calculated by CMG-GEM for cores #4 and 5 are shown by Figs. 6 and 7, respectively. The Carman-Kozeny exponents used in these calculations were 4.53 when seawater without sulfate injected with CO_2 during WAG injection, and 7.82 in the seawater case (Mohamed and Nasr-El-Din 2012).

Fig. 6 shows that for core #4 an enhancement in the permeability was noted close to the core inlet until 1.5 in. from the core inlet; more increase in the permeability was noted in each cycle. Behind this region, damage was noted at the core outlet, and the damage increased with the number of WAG cycles. Seawater in CO_2 WAG injection causes a reduction in core permeability throughout the core length, with more damage close to the core inlet due to calcium sulfate precipitation (Fig. 7). The damage increases as more WAG cycles are injected.

TABLE 6 A SUMMARY OF THE REACTION RATE CONSTANTS FOR EACH BRINE USED IN THIS STUDY

Brine	Log (k_{25}) mol/m^2.s	Maximum Calcium Concentration Measured mg/l	Maximum Calcium Concentration Simulated mg/l
DI Water	-9.20	1,184	1,168
1 wt% NaCl	-9.08	1,276	1,264
5 wt% NaCl	-7.38	1,841	1,788
10 wt% NaCl	-7.30	1,700	1,724
1 wt% $MgCl_2$	-7.3	1,764	1,776
5 wt% $MgCl_2$	-7.05	2,686	2,672
10 wt% $MgCl_2$	-6.55	2,843	2,832
1 wt% $CaCl_2$	-7.72	[a]4,256	4,276
5 wt% $CaCl_2$	-6.20	[b]22,792	23,000
Seawater without sulfate	-6.70	[c]2,300	2,240
Seawater	-6.46	1,780	1,800

a initial calcium concentration = 3,100 mg/l
b initial calcium concentration = 15,504 mg/l
c initial calcium concentration = 401 mg/l

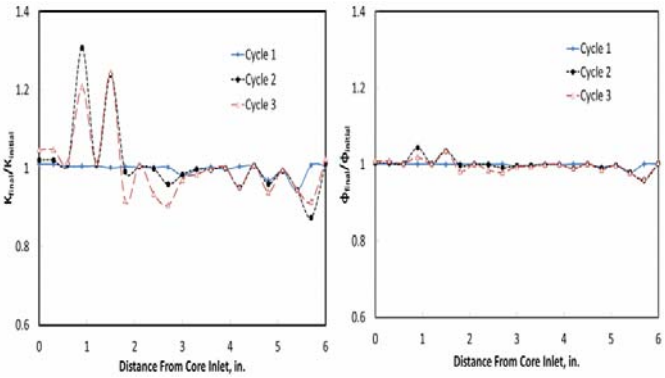

FIG. 6 PERMEABILITY AND POROSITY RATIOS AT THE END OF EACH WAG CYCLE WHEN WAG INJECTION OF CO_2 AND SEAWATER WITHOUT SULFATE CONDUCTED FOR CORE #4.

The overall core permeability after WAG injection for cores #4 and 5 is given in Fig. 8. Most of the change in permeability occurs during the first WAG cycle, the permeability after the second and third WAG cycle was almost the same as after the first cycle. A good match between the permeability measured in the lab and calculated by the simulator was also shown in Fig. 8.

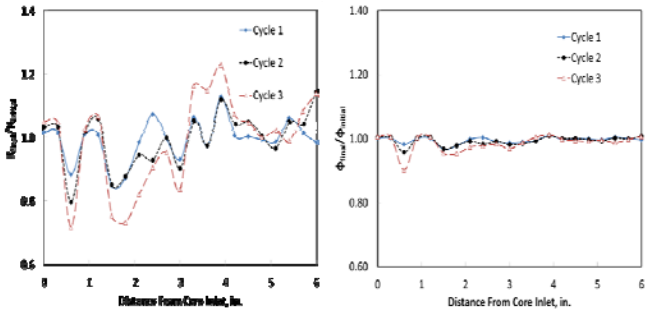

FIG. 7 PERMEABILITY AND POROSITY RATIOS AT THE END OF EACH WAG CYCLE WHEN WAG INJECTION OF CO_2 AND SEAWATER CONDUCTED FOR CORE #5.

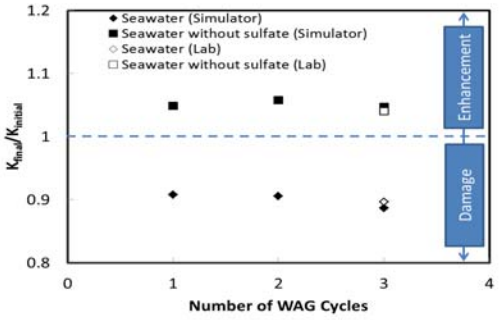

FIG. 8 COMPARISON BETWEEN THE PERMEABILITY DATA OBTAINED FROM THE SIMULATOR AND MEASURED IN THE LAB FOR CORES #4 AND 5.

A. *Field Scale Simulation*

Simulation in the field scale was conducted based on the reaction kinetics obtained from the core scale simulations. The aquifer model is a homogenous saline aquifer with dimensions of 10 km X 10 km X 50 m in the x, y, and z directions, respectively. The aquifer is 2500 m deep with a temperature of 163°F. The porosity is 0.15, horizontal permeability of 100 mD, and vertical permeability of 33 mD. The aquifer was initially at normal pore pressure gradient of 0.465 psi/ft (Dahle et al. 2009).

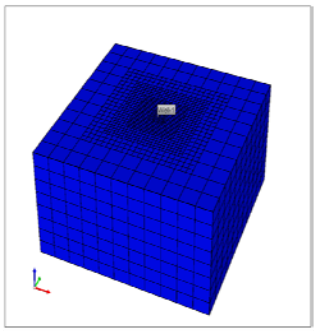

Property	Value
length	10 km
width	10 km
thickness	50 m
depth	2500 m
T	163°F
ϕ	0.15
k_h	100 mD
k_v	33 mD

FIG. 9 AQUIFER MODEL USED IN THE SIMULATION STUDY.

The aquifer was divided into Cartesian grids with 11X11X8 blocks in x, y, and z directions, with refining the grids into smaller blocks as we move toward the injector (Fig. 9). The injection well was completed at the center of the aquifer. Injection was conducted at a constant bottomhole pressure of 5740 psi (equivalent to a fracture pressure gradient of 0.7 psi/ft). The simulator ran for 30 years of CO_2 injection, and 1400 years after injection (the maximum number of time steps reached) to monitor the movement of CO_2 and the changes in trapping mechanisms. The aquifer was initially saturated with formation brine with the composition given in Table 4. WAG injection of CO_2 was conducted in each cycle which was composed of 9 months of CO_2 injection and 3 months of brine injection. Three brines were tested;

a) DI Water

b) Seawater without sulfate

c) Seawater

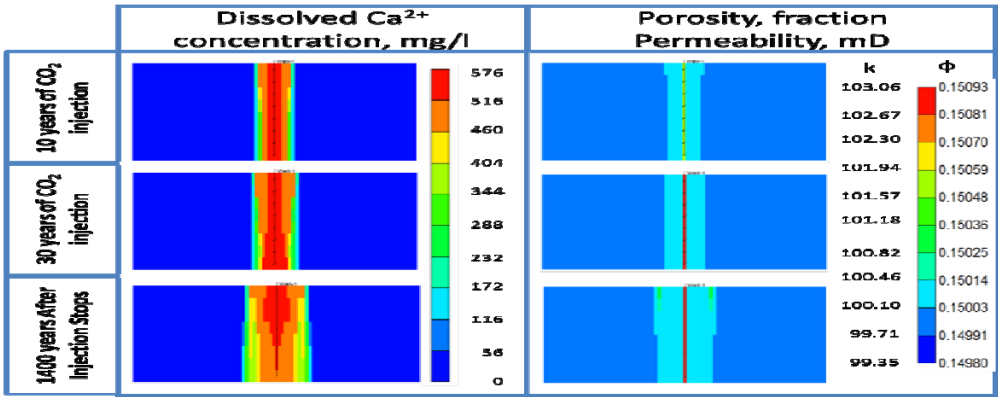

FIG. 10 DISTRIBUTION OF POROSITY, PERMEABILITY AND THE DISSOLVED CALCIUM IN THE AQUIFER AFTER 10 YEARS OF WAG INJECTION OF CO_2 AND DI WATER, AT THE END OF INJECTION, AND 1400 YEARS AFTER INJECTION STOPS.

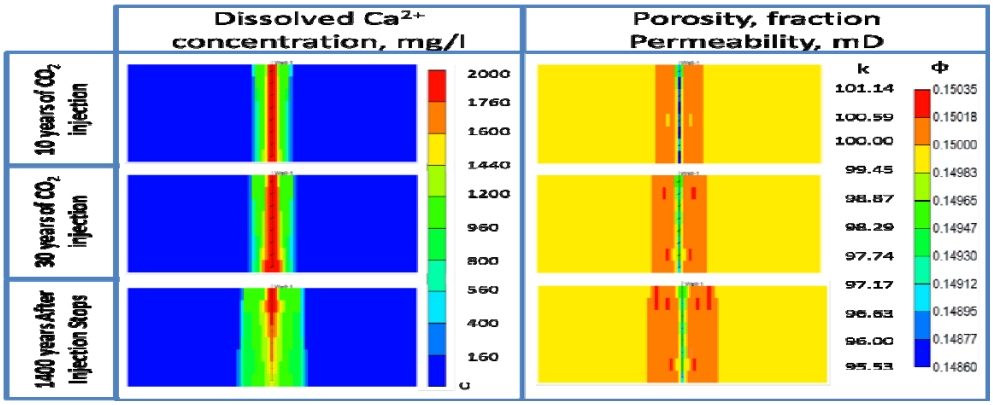

FIG. 11 DISTRIBUTION OF POROSITY, PERMEABILITY AND THE DISSOLVED CALCIUM IN THE AQUIFER AFTER 10 YEARS OF WAG INJECTION OF CO_2 AND SEAWATER WITHOUT SULFATE, AT THE END OF INJECTION, AND 1400 YEARS AFTER INJECTION STOPS.

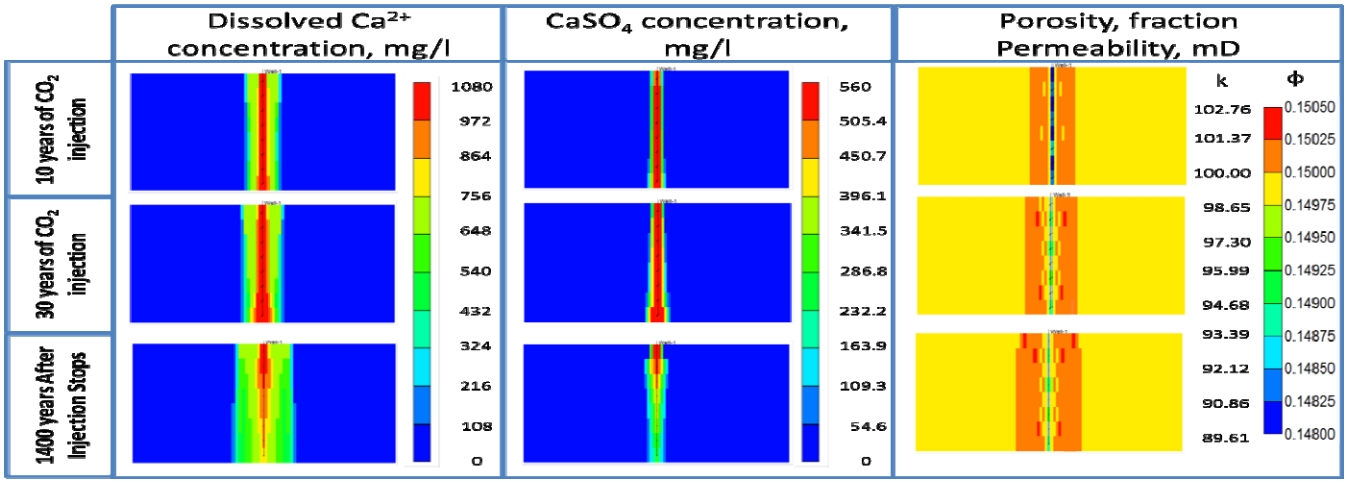

FIG. 12 DISTRIBUTION OF POROSITY, PERMEABILITY AND THE DISSOLVED CALCIUM IN THE AQUIFER AFTER 10 YEARS OF WAG INJECTION OF CO_2 AND SEAWATER, AT THE END OF INJECTION, AND 1400 YEARS AFTER INJECTION STOPS.

The amount of CO_2 injected for each case was almost the same. The cumulative CO_2 injected was 2.7 mega ton with 809,448 m^3 DI water for the first case, 2.63 mega ton with 794,844 m^3 seawater without sulfate for the second case, and 2.63 mega ton with 790,931 m^3 seawater for the third case. The values give a storage efficiency of 0.5% (total volume of CO_2 injected at reservoir conditions divided by the total pore volume of the aquifer, which equals 750,000,000 m^3).

The permeability and porosity distributions in the aquifer during WAG injection of CO_2 and 1400 years after injection stops are shown in Figs. 10-12. The dissolved calcium and calcium sulfate concentration (for the seawater case) are also shown in these figures. The main changes in the permeability occurred within the wellbore block grids, beyond these blocks a minor change in porosity and permeability was noted.

For the DI water case (Fig. 10) no damage was observed (no precipitation occurred). The dissolved calcium concentration shows that the maximum calcium concentration was 580 mg/l because of the small reaction rate constant (-9.2) as shown in Table 6. The maximum increase in the permeability was 3 mD around the wellbore region.

WAG injection of CO_2 and seawater without sulfate caused a 5 mD loss in the permeability around the wellbore (Fig. 11) after 10 years of injection due to the precipitation of calcium carbonate. At the end of injection (after 30 years) the damage reduced due to the rock dissolution, the final reduction in permeability was only 2 mD. The maximum dissolved calcium concentration was 2000 mg/l. The enhancement in permeability in the DI water case and damage in the seawater without sulfate case still insignificant, the change in permeability didn't exceed 5%.

More damage was observed in WAG injection of CO_2 with seawater, a 10 mD loss in permeability after 10 years of injection occurred, due to precipitation of calcium sulfate. Fig. 12 shows that the formation of

calcium sulfate occurred in this case and the calcium sulfate concentration increased to 560 mg/l.

Fig. 13 shows the contribution of each trapping mechanism to keep CO_2 in place over time. Table 7 shows that brine composition does not affect the trapping contribution of each trapping mechanism and the values are close for the three cases tested in this study.

Most of CO_2 was trapped as a free phase, and it contributes more than 40 mol% after 1400 years since the injection stopped. Fig. 13 shows that amount of free gases decreases with time, due to upward migration of CO_2 because of the gravity difference, leaving behind CO_2 trapped in residual phases; also more CO_2 is dissolved in the aquifer brine with time.

TABLE 7 TRAPPED PHASES AFTER WAG INJECTION OF CO_2 INTO SALINE CARBONATE AQUIFER

Brine Composition		DI Water	Seawater without Sulfate	Seawater
0 years after injection stops	Free CO_2 mol%	67.55	68.33	68.55
	Residual CO_2 mol%	15.94	15.23	15.48
	Dissolved CO_2 mol%	12.45	12.38	12.41
1400 years after injection stops	Free CO_2 mol%	42.91	43.77	43.73
	Residual CO_2 mol%	21.98	21.64	21.77
	Dissolved CO_2 mol%	34.47	33.90	34.05

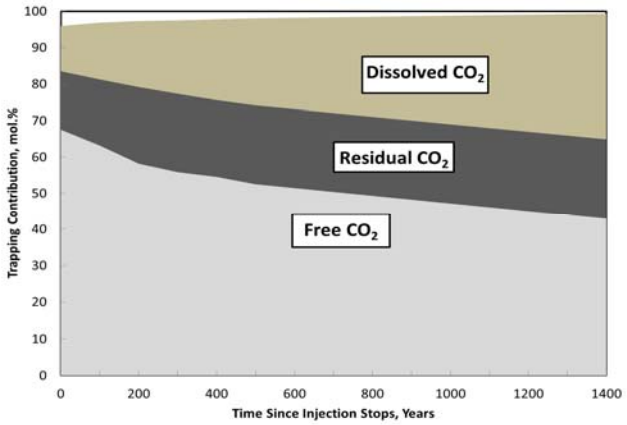

FIG. 13 TRAPPED PHASES AFTER WAG INJECTION OF CO_2 AND SEAWATER WITHOUT SULFATE INTO SALINE CARBONATE AQUIFER.

Conclusions

Brine composition is a critical factor that affects the chemical reactions between CO_2/brine/rock during CO_2 sequestration in carbonate aquifers. Different brine compositions, temperatures, and injection flow rates were examined. The study pertains mostly to limestone saline aquifers. A commercial reservoir simulator (CMG-GEM) was used to predict lab data and field results. Based on the results obtained, the following conclusions can be drawn:

1) Injection of lower salinity brines with CO_2 in WAG injection wells maintains the well injectivity and allows higher injection flow rate of CO_2 to be injected over time. The simulator predicted an enhancement in the permeability in the near wellbore region when DI water was injected with CO_2, while 5 mD reduction in the permeability in the near wellbore region was predicted when seawater without sulfate was injected with CO_2.
2) Using low sulfate brines is highly recommended in WAG injection projects to reduce the magnitude of damage in the near wellbore region. Up to 11 mD reduction in the permeability was noted when seawater was injected with CO_2.
3) Calcium chloride has the most significant effect on the limestone cores during sequestration, and increasing calcium chloride concentration caused a significant increase in calcium concentration in the core effluent samples.
4) A higher reaction rate constant ($\log(k_{25})$) was predicted as the brine salinity increased to simulate the increase in calcium concentration observed in the core effluent samples.
5) Based on the simulator results, the amount of CO_2 trapped in each trapping phase (free, residual, and dissolved) was almost the same regardless of the brine composition.

ACKNOWLEDGMENT

The authors would like to thank Texas Engineering Experiment Station (TEES) at Texas A&M University, Crisman Institute Petroleum Research for funding this work. Ms. K. Brady is acknowledged for proof reading this paper.

REFERENCES

Alkattan, M., Oelkers, E.H., Dandurand, J.L., Schott.J. 1998. An experimental study of calcite and limestone dissolution rates as a function of pH from -1 to 3 and temperature from 25 to 80°C. *Chemical Geology* **151**(1): 199–214.

Alotaibi, M.B., Nasralla, R.A., Nasr-El-Din, H.A., 2010. Wettability Challenges in Carbonate Reservoirs. Paper SPE 129972 presented at Improved Oil Recovery Symposium held in Tulsa, Oklahoma, 24-28 April.

Bacon, D.H., Sass, B.M., Bhargava, M., Sminchak, J. and Gupta, N. 2009. Reactive Transport Modeling of CO_2 and SO_2 Injection into Deep Saline Formations and Their Effect on the Hydraulic Properties of Host Rocks. *Energy Procedia* **1** (1) 3283–3290.

Bethke, C.M. 1996. Geochemical Reaction Modeling. Oxford University Press, New York.

Boving, T.B. and Grathwohl, P., 2001, Tracer diffusion coefficients in sedimentary rocks: correlation to porosity and hydraulic conductivity, *Journal of Contaminant Hydrology*, **53**(1): 85-100.

Cantucci, B., Montegrossi, G., Vaselli, O., Tassi, F., Quattrocchi, F., and Perkins E.H. 2009. Geochemical modeling of CO_2 storage in deep reservoirs: The Weyburn Project (Canada) case study. *Chemical Geology* **265** (1) 181–197.

Dahle, H.K., Eigestad, G.T., Nordbotten, J.M., and Pruess K. 2009. A Model-Oriented Benchmark Problem for CO_2 Storage. Workshop on Modeling and Risk of Assessment of Geological Storage of CO_2.

Duan, Z., Sun, R., Zhu, C., and Chou, I.M., 2006. An improved model for the calculation of CO_2 solubility in aqueous solutions containing Na^+, K^+, Ca^{2+}, Mg^{2+}, Cl^-, and SO_4^{2-}. *Marine Chemistry* **98** (2): 131–139.

Egermann, P., Bazin, B., and Vizika, O. 2005. An Experimental Investigation of Reaction-Transport Phenomena during CO_2 Injection. Paper SPE 93674 presented at the SPE Middle East Oil & Gas Show and Conference held in Bahrain, 12–15 March.

El-Khatib, N. 1995. Development of a Modified Capillary Pressure J-Function. Paper SPE 29890 presented at Middle East Oil Show, Bahrain, 11-14 March.

Enick, R.M., and Klara, S.M., 1989. CO_2 Solubility in Water and Brine Under Reservoir Conditions. *Chemical Engineering Communications* **90**(1): 23-33.

Flint, O., 1967. Increased Solubility of Calcium Sulphate in Sea Water Containing Hydrochloric Acid. *Desalination* **4**(3): 28-335.

Gaus, I., Azaroual, M., and Czernichowski-Lauriol, I. 2004. Reactive transport modeling of the impact of CO_2 injection on the clayey cap rock at Sleipner (North Sea). *Chemical Geology* **217** (3): 319– 337.

Grigg, R.B., and Svec, R.K., 2008. Injectivity Changes and CO_2 Retention for EOR and Sequestration Projects. Paper SPE 110760 presented at the SPE/DOE Improved Oil Recovery Symposium held in Tulsa, Oklahoma, U.S.A., 19-23 April.

Knauss, K.G., Johnson, J.W., and Steefel, C.I. 2005. Evaluation of the impact of CO_2, co-contaminant gas, aqueous fluid and reservoir rock interactions on the geologic sequestration of CO_2. *Chemical Geology* **217** (3): 339–350.

Krumhansl, J., Pawar, R., Grigg, R., Westrich, H., Warpinski1, N., Zhang, D., Jove-Colon1, C., Lichtner, P., Lorenz, J., Svec, R., Stubbs, B., Cooper, S., Bradley, C., Rutledge, J., and Byrer C., 2002. Geological Sequestration of Carbon Dioxide in a Depleted Oil Reservoir. Paper SPE 75256 presented at the SPE/DOE Improved Oil Recovery Symposium held in Tulsa, Oklahoma, 13–17 April.

Lee,Y.-J and Morse, J.W. 1999. Calcite precipitation in synthetic veins: Implications for the time and fluid volume necessary for vein filling. *Chemical Geology* **156** (1): 151–170.

Linnikov, O.D. and Podbereznyi, V.L., 1996. Prevention of sulfate scale formation in desalination of Aral Sea water. *Desalination* **105** (1): 143-150.

Marshall, W.L. and Slusher, R., 1968. Aqueous Systems at High Temperature. Solubility to 200°C of Calcium Sulfate and Its Hydrates in Seawater and Saline Water Concentrates, and Temperature-Concentration Limits. *J. Chem. Eng. Data* **13**(1); 83-93.

Meijer, J.A.M. and Van Rosmalen, G.M., 1984. Solubilities and Supersaturations of Calcium Sulfate and its Hydrates in Seawater. *Desalination*, **51** (3): 255-305.

Mohamed, I.M. and Nasr-El-Din, H.A. 2012. Permeability Alternation and Trapping Mechanisms during CO_2 Injection in Homogenous Limestone Aquifers: Lab and Simulation Studies. *Canadian Energy Technology and Innovation Journal* **1** (1):41-55.

Mohamed, I.M., and Nasr-El-Din, H.A. 2012. Formation Damage Due to CO_2 Sequestration in Deep Saline Aquifers. SPE 151142 presented at SPE International Symposium & Exhibition on Formation Damage Control held in Lafayeete, Louisiana, USA, 15–17 February.

Nighswander, J.A., Kaiogerakis, N., and Mehrotra, A.K., 1989. Solubilities of Carbon Dioxide in Water and 1 wt% NaCl Solution at Pressures up to 10 Mpa and Temperatures from 80 to 200°C. *J. Chem. Eng. Data* **34**(3): 355-360.

Partridge, E.P., and White, A.H., 1929. The Solubility of Calcium Sulfate from 0 to 200°, *J. Am. Chem. Soc*., **51**(2): 360-370.

Prutton, C.F., and Savage, R.L. 1945. The Solubility of Carbon Dioxide in Calcium Chloride-Water Solutions at 75, 100, 120° and High Pressures. *J. Am. Chem. Soc*. **67**(9): 1550–1554.

Raistrick, M., Hutcheon, I., Shevalier, M., Nightingale M., Johnson, G., Taylor, S., Mayer, B., Durocher, K., Perkins, E., and Gunter, B., 2009. Carbon dioxide-water-silicate mineral reactions enhance CO_2 storage; evidence from produced fluid measurements and geochemical modeling at the IEA Weyburn-Midale Project. *Energy Procedia* **1** (1): 3149–3155.

Shariat, A., Moore, R.G., Mehta, S.A., Van Fraassen, K.C., Newsham, K.E. and Rushing, J.A. 2012. Laboratory Measurements of CO_2-H_2O Interfacial Tension at HP/HT Conditions: Implications for CO_2 Sequestration in Deep Aquifers. Paper CMTC 150010 presented at the Carbon Management Technology Conference, Orlando, Florida, 7-9 February.

Sorensena, J.A., Holubnyaka, Y.I., Hawthornea, S.B., Millera, D.J., Eylandsa, K., Steadmana, E.N., and Harjua, J.A. 2009. Laboratory and numerical modeling of geochemical reactions in a reservoir used for CO_2 storage. *Chemical Geology* **265** (1):181-197.

Svensson, U., and Dreybrodt, W. 1992. Dissolution kinetics of natural calcite minerals in CO_2–water systems approaching calcite equilibrium. *Chemical Geology* **100**(1): 129-145.

Wellman, T.P., Grigg, R.B., McPherson, B.J., Svec, R.K., and Lichtner, P.C. 2003. Evaluation of CO_2-Brine-Reservoir Rock Interaction with Laboratory Flow Tests and Reactive Transport Modeling. Paper SPE 80228 presented at the SPE International Symposium on Oilfield Chemistry held in Houston, Texas, 5-7 February.

Wigand, M., Carey, J.W., Schütt, H., Spangenberg, E., and Erzinger, J. 2009. Geochemical effects of CO_2 sequestration in sandstones under simulated in situ conditions of deep saline aquifers. *Applied Geochemistry* **23** (9): 2735–2745.

Xu, T., Sonnenthal, E., Spycher, N., and Pruess, K. 2006. TOUGHREACT—A simulation program for non-isothermal multiphase reactive geochemical transport in variably saturated geologic media: Applications to geothermal injectivity and CO_2 geological sequestration. *Computers & Geosciences* **32** (2): 145–165.

Ibrahim M. Mohamed is a senior geomechanics engineer at Advantek International, Houston, Texas. He received his B.Sc. and M.Sc. degrees from the Petroleum Engineering Department at Cairo University, Egypt. And he received his PhD degree from Petroleum Engineering Department at Texas A&M University. His areas of research include well stimulation and formation damage removal, CO_2 injection, waste disposal and pressure transient analysis. He has published and presented more than 20 technical papers.

Jia He is a PhD candidate at Texas A&M University in petroleum engineering. Email: jia.he@pe.tamu.edu. His research interests include oil filed scale prediction and chemical treatments, CO_2 sequestration, cost effective acidizing treatments, and innovative acid fracturing studies. He has published several papers. He holds a BE degree from Eastern China University of Petroleum and MS degree from Texas A&M University, both in Petroleum Engineering.

Dr. Hisham A. Nasr-El-Din is a professor and holder of the John Edgar Holt Endowed Chair at Texas A&M University in Petroleum Engineering. Previously, he worked for 15 years as Principal Professional and Team Leader of the Stimulation Research and Technology Team, Saudi Aramco. Before joining Saudi Aramco, he worked for four years as a staff research engineer with the Petroleum Recovery Institute in Calgary. He also worked as a research associate with the University of Saskatchewan, the University of Ottawa and the University of Alberta, all in Canada. His research interests include well stimulation, formation damage, enhanced oil recovery, conformance control, interfacial properties, adsorption, rheology, cementing, drilling fluids, two-phase flow and non-damaging fluid technologies. Nasr-El-Din has several patents and has published and presented more than 480 technical papers. He has received numerous awards within Saudi Aramco for significant contributions in stimulation and treatment-fluid technologies and stimulation design, and for his work in training and mentoring. Nasr-El-Din holds B.Sc. and M.Sc. degrees from Cairo University, Egypt and a Ph.D. degree from the University of Saskatchewan, Canada, all in Chemical Engineering.